Electronic and magnetic structure of a Cr monolayer on Ag(100)

C. Krembel, M. C. Hanf, J. C. Peruchetti, D. Bolmont, and G. Gewinner
Laboratoire de Physique et de Spectroscopie Electronique, 4 rue des Frères Lumière, 68093 Mulhouse CEDEX, France
(Received 11 April 1991)

Angle-resolved photoemission is used to study the electronic structure of the Cr layers obtained by condensing one layer equivalent (LE), or less, of Cr on Ag(100) at low ($\sim$0.5 LE/min) deposition rates. The data confirm our earlier finding that, upon deposition on a mildly ($\sim$440 K) heated substrate, layer-by-layer growth takes place up to 1 LE, i.e., an ordered flat Cr monolayer with a good degree of perfection is formed. The substrate temperature during deposition is critical since lower ($\sim$300 K) or higher ($\sim$500 K) temperatures result in an inhomogeneous rough Cr layer. For the ordered flat monolayer the characteristic two-dimensional dispersion of the Cr 3*d* energy bands and their symmetry at $\bar{\Gamma}$ is determined. It is argued that when considered together with electron-diffraction observations, which reveal a weak $c(2\times2)$ pattern at low energies ($\leq$30 eV), the photoemission results provide compelling evidence of a monolayer stabilized by antiferromagnetic order. The large energy gap at the Fermi energy indicates that the effect must be very strong with a local moment in the range $(3-4)\mu_B$, as predicted theoretically.

I. INTRODUCTION

The ability to prepare ultrathin metal films has recently generated a great deal of interest in their structural, electronic, and magnetic properties, which are possibly radically different from their bulk counterparts. For example, lattice spacings different from the bulk,[1,2] two-dimensional (2D) electronic states,[1] and anomalous magnetic properties[1,3] have been reported. Monolayers of 3*d* transition metals are of particular interest, since theory predicts strong 2D magnetic arrangements even for weakly magnetic or nonmagnetic metals such as Cr and V.[4,6] For a Cr monolayer on[5] Au(100) or[6] Pd(100) a $c(2\times2)$ antiferromagnetic structure with a large local moment ($\sim3.50\mu_B$) is found to be the most stable configuration. These predictions are consistent with the general tendency of the metals in the middle of the transition-metal series toward antiferromagnetism or structures based on a twofold superlattice.[7] From an experimental point of view the characterization and preparation of flat ordered monolayers of 3*d* metals with a sufficient degree of perfection is reportedly a difficult task. It is interesting to select a noble-metal substrate to reduce the overlayer-substrate interaction, but unfortunately the relative surface energies do not favor the growth of a flat monolayer. Previous work shows that alloying occurs for the Cr/Au(100) system even at room temperature (RT).[8] On the other hand, bilayers are apparently formed above $\sim$0.3 layer equivalent (LE) for deposition on Ag(100) held at RT.[9,10] Nevertheless, we recently succeeded in preparing a flat ordered Cr monolayer on Ag(100) by deposition on a mildly heated (440 K) substrate as evidenced by photoelectron forward-scattering measurements and bare Ag(100) planimetry in the submonolayer range.[10] However, higher (>460 K) substrate temperatures either during or after deposition invariably induce Cr agglomeration into 3D islands, as expected from thermodynamics. Possible reasons for this unusual growth mode will be discussed elsewhere in conjunction with appropriate experiments.[11]

The above findings provide the unique opportunity to investigate the properties of a Cr monolayer expected to be a very interesting realization of 2D magnetism. In this respect, the present paper reports selected photoemission experiments that probe the Cr 3*d* valence states and Cr 2*p* core level, i.e., the electronic structure of the layers in the monolayer range. First, the data confirm the conclusion drawn from structure-sensitive methods in Ref. 10 that Cr deposited on Ag(100) kept at 440 K grows in the form of 2D islands up to 1 LE. These islands exhibit a good degree of order with characteristic Cr 3*d* electronic states and a 2D band structure. In contrast, RT deposition results in a badly ordered inhomogeneous layer. Second, along with low-energy-electron-diffraction (LEED) observations, the photoemission results provide strong evidence that the ordered monolayer is actually stabilized by $c(2\times2)$ antiferromagnetic order with a large local magnetic moment.

The outline of the paper is as follows. Section II is concerned with experimental details. Section III A summarizes our LEED observations in the monolayer range. Section III B presents selected valence-band and Cr 2*p* core-level photoemission data for various Cr layers in the submonolayer range deposited at different substrate temperatures. The main purpose of this section is to establish a relationship between electronic and atomic structure of the layer and, in addition, to check the validity of the growth mode reported in Ref. 10. Section III C is devoted to a more detailed angle-resolved-photoemission study of the electronic structure of the ordered Cr monolayer obtained by deposition at 440 K. This extends and confirms our previous preliminary work.[12] In Sec. III D we discuss the LEED and photoemission data from the ordered monolayer, and Sec. IV contains the conclusion.

II. EXPERIMENT

The experiments were performed in an UHV chamber equipped with low-energy electron diffraction (LEED) and angle-resolved ultraviolet and x-ray photoelectron spectroscopy techniques. For measurements of the valence band the 50-mm hemispherical analyzer was usually operated at a pass energy of 5 eV. The acceptance cone of $\sim 3°$ provides then an energy resolution of 100–150 meV for He I photons. In core-level measurements the resolution is limited to ~ 1 eV because of the natural linewidth of the Mg $K\alpha$ or Al $K\alpha$ x-ray source. All photoemission data presented in this paper are collected with the sample at RT, irrespective of the substrate temperature during film growth, and as quickly as possible after deposition in order to minimize possible rearrangements in the overlayer due to surface diffusion.

The Ag(100) crystal was mechanically and chemically polished by standard methods. In practice, the preparation of a good surface is fairly difficult, since only one out of several attempts usually gives a good polish. Sizable effects on the growth mode were occasionally observed on surfaces with a large number of defects. The crystal was cleaned *in situ* by Ar-ion sputtering and annealing at 500 °C until a clean (as judged by photoemission) Ag(100) surface with a sharp $p(1\times1)$ LEED pattern was obtained. Cr was evaporated from a source operating at a rate of ~ 0.5 LE/min and a base pressure of 2×10^{-10} Torr. One layer equivalent (LE) corresponds to the Ag(100) or Cr(100) surface atomic densities which are essentially the same, since there is a nearly perfect match in surface translation vectors. Apparently, no impurities were codeposited from this source. An accurate determination of the absolute Cr coverage is particularly important in this kind of experiment. A careful calibration of the quartz balance was achieved by mounting a second quartz balance in the sample position in order to determine the geometric correction factor. In the monolayer range the accuracy is about $\pm 10\%$. This was cross-checked by Cr $2p_{1/2}$ and Ag $3d$ core-level intensity measurements. One LE is found to correspond to a Cr $2p_{1/2}$ to Ag $3d$ signal-height ratio of 0.016 for collection at a polar angle of 45° in a Ag(010) plane. This is in reasonable agreement with estimations based on published photoionization cross sections and inelastic mean free paths of electrons in Ag.

III. RESULTS AND DISCUSSION

A. LEED observations

By 1 LE deposited at RT the LEED pattern remains $p(1\times1)$, but the quality of the diagram, i.e., the signal-to-noise ratio and diffracted beamwidth show a small but sizable deterioration with respect to clean Ag(100). No similar worsening is observed when deposition is achieved at 440 K since a low background pattern comparable to clean Ag(100) is still visible by 1 LE. Typical changes in the $I(E)$ curves reflect scattering from a Cr overlayer. This is consistent with the formation of an ordered Cr monolayer at 440 K as established in Ref. 10. The most important observation here is that while the pattern is $p(1\times1)$ for beam energies $E \geq 30$ eV, a weak $c(2\times2)$ superstructure is visible at low energies $E \leq 30$ eV. At normal incidence, the intensity of the $(\frac{1}{2}\frac{1}{2})$ spots passes through a maximum near $E=26$ eV. Spot photometer measurements show that this maximum intensity of the half-order spots is remarkably reproducible about 0.15% and 2% of the (00) and (10) spots, respectively. In particular, no correlation with chemisorbed impurities could be evidenced. For instance, exposure to oxygen results in a progressive worsening of the whole pattern but no enhancement of the half-order spots could be detected. Moreover, if the superstructure were due to a small contamination of the surface it seems very difficult to understand why it is not detected at all above $E \sim 30$ eV. Hence, this is apparently an intrinsic phenomenon characteristic of the flat ordered Cr monolayer. The extra spots are visible up to 430 K and exhibit a remarkable stability over several hours in UHV. We were not able to clearly identify a similar superstructure on Ag(100) coated with 1 LE deposited at RT.

B. Electronic structure and mode of growth

Figure 1 shows typical angle-resolved-photoemission spectra collected in the Ag(010) plane at a polar angle $\theta=55°$ (referred to the surface normal) with $\hbar\omega=21.2$-eV

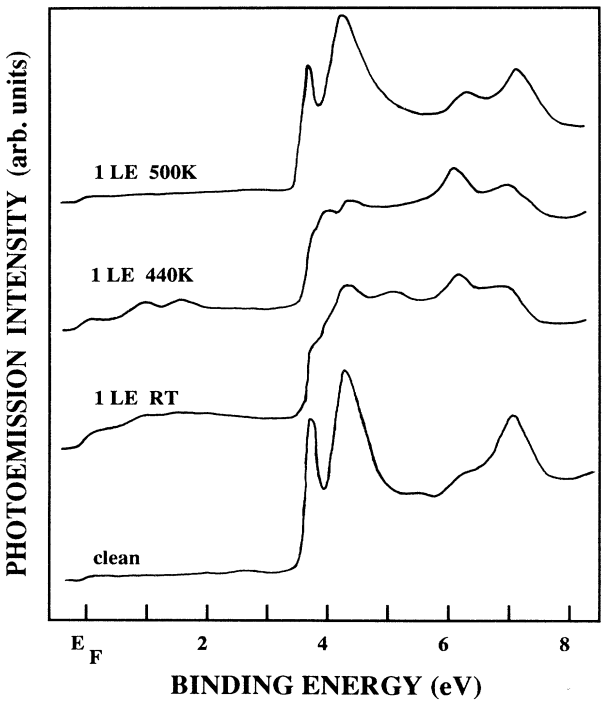

FIG. 1. Angle-resolved-photoemission spectra collected in the Ag(010) plane at a polar angle $\theta=55°$, referred to the surface normal, with He I radiation. The data for clean Ag(100) and for 1 LE of Cr deposited at RT, 440, and 500 K are presented. Note the appearance of Cr $3d$ structures in the large featureless spectral region extending from top edge of the Ag $4d$ bands at ~ 3.8 eV up to the Fermi energy.

excitation. Prominent structures in the 3.8–8-eV binding-energy (BE) range reflect emission from Ag 4*d* valence band. For clean Ag(100) the narrow feature near 3.80-eV BE is a Tamm-like surface state at $\bar{M}$, the symmetry point of the surface Brillouin zone (SBZ) probed in the present collection geometry.[13] As can be seen, for clean Ag(100), there is a wide BE window of ~3.5 eV below E_F, where the spectrum is just a very low featureless background due to incoherent emission from the wide Ag 5*s* band. The small bumps near 2 and 2.7 eV are due to a satellite of the He I radiation. Direct transition features from Ag 5*s* band can be identified for some particular collection geometries, but usually no structured emission from substrate is observed in this spectral region. This is a very favorable situation, since the Cr 3*d* features are expected to appear in this BE window, and overlap with substrate emission would considerably obscure the spectral interpretation. The latter problem is particularly evident in recent calculations of photoemission from 3*d*-metal layers on Pd(100).[14]

Figure 1 shows that for 1 LE of Cr deposited on Ag(100) at 440 K, the surface state completely disappears and two well-resolved Cr 3*d* features at 1.07 and 1.75 eV attest to the presence of the Cr. Note that the Cr 3*d* states reflect in particularly narrow features, about 300 meV full width at half maximum (FWHM). This is attributed to the formation of an ordered Cr monolayer characterized by well-defined electronic states. Figure 2 displays an enlarged view of the relevant BE window for 0.5 and 1 LE deposited at 440 K. It can be seen that

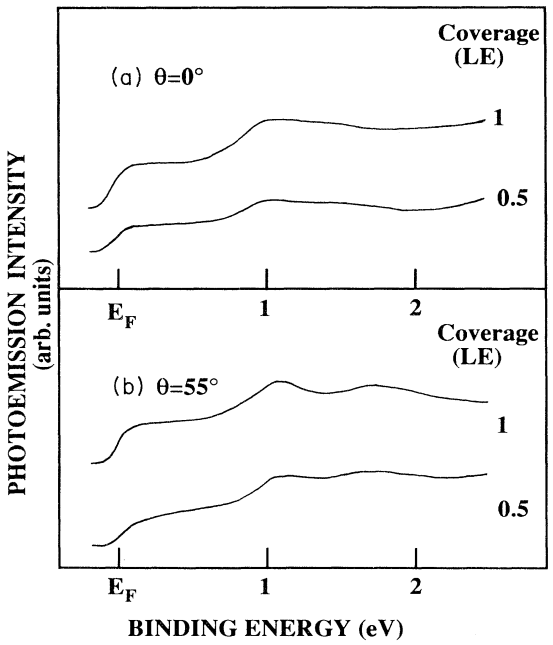

FIG. 2. Enlarged view of the Cr 3*d* induced features in the 0–2-eV spectral region. Same photon energy and collection plane as in Fig. 1. (a) Normal- ($\theta=0°$) and (b) off-normal- ($\theta=55°$) emission data are shown for 0.5 and 1 LE of Cr deposited at 440 K.

whatever the collection geometry the overall shape and energy location of the spectral features are exactly the same for both coverages. At normal emission the Cr 3*d* induced structures at 1.07 and ~1.5 eV are not so well resolved than at $\theta=55°$, but in both cases we observe that their intensity at 1 LE is essentially twice as large as at 0.5 LE. More generally we find that the intensity increases linearly with coverage in the 0.2–1-LE range. This indicates that the Cr grows in the form of ordered 2D islands which eventually cover the whole surface near 1 LE. Moreover, no sizable change in peak width is observed as a function of coverage above ~0.3 LE, where a reasonably accurate estimation can be made. This suggests that island edge effects are small, and in turn that the island diameter is large with respect to the surface lattice spacing, in agreement with the conclusion of Ref. 10 that a small density of large islands must be formed at 440 K. The high mobility of the adatoms at these temperatures favors the formation of large islands.

A markedly different behavior is found for deposition at lower or higher substrate temperatures during growth. It can be seen in Fig. 1 that deposition of 1 LE at 500 K only quenches about 30% of the surface-state intensity and increases the background emission in the 0–3.5-eV BE range. There is no evidence of any distinct Cr 3*d* feature. This suggests a drastic agglomeration of the Cr at higher temperatures leaving about 70% of clean Ag (100). The Cr is still detectable by Cr 2*p* core-level emission indicating the presence of 3D Cr islands, which have apparently a featureless valence-band signature. On the other hand, Fig. 1 shows that deposition at RT results in a spectrum which resembles the one obtained at 440 K. The surface state is practically suppressed and two Cr 3*d* induced features are visible about 1.07 and 1.75 eV, but they are small, not well resolved, and fairly broad. According to the 440-K data this indicates that monolayer islands are also formed at RT, but apparently they are poorly ordered and probably small in size. Again, this is consistent with the conclusion arrived at in Ref. 10 that a large density of small islands is formed at RT, probably because of a limited adatom mobility. From data similar to those of Fig. 1 we can roughly estimate the fraction of the total surface (assumed to be proportional to the intensity of the Cr 3*d* features) covered by such monolayer islands to be ~50% for 1 LE deposited at RT. The remainder of the Cr must be present in the form of bilayers or multilayers. Yet the photoemission signature of this kind of Cr seems not clearly apparent in the RT spectrum of Fig. 1. Note, however, the enhanced emission near the Fermi level with respect to the 440-K spectrum. In this respect let us now consider the details of the Cr 3*d* region at normal emission for RT deposition, shown in Fig. 3. For 1 LE deposited at RT we can identify two broad features at 1.05 and 1.5 eV, which, according to the data of Fig. 2, confirm the presence of monolayer platelets. However, interestingly, there is additional strong emission near E_F with a typical broad feature about 0.45 eV. This must reflect the emission from Cr incorporated in bilayer or multilayer platelets, i.e., Cr in a more bulklike environment. Detailed studies for coverages above 1 LE clearly confirm this assignment.[11] It is

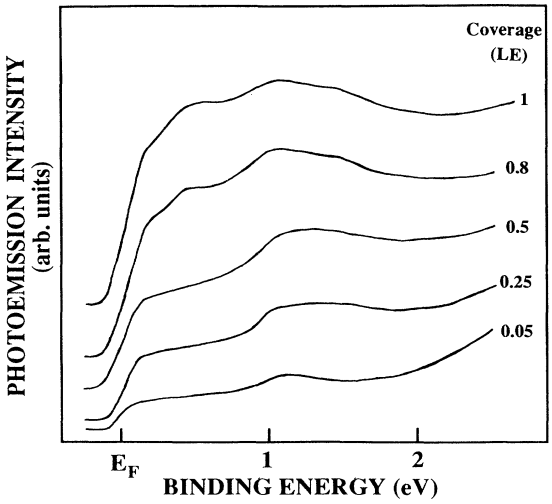

FIG. 3. Same as Fig. 2 at normal emission but for various amounts in the submonolayer range of Cr deposited at RT.

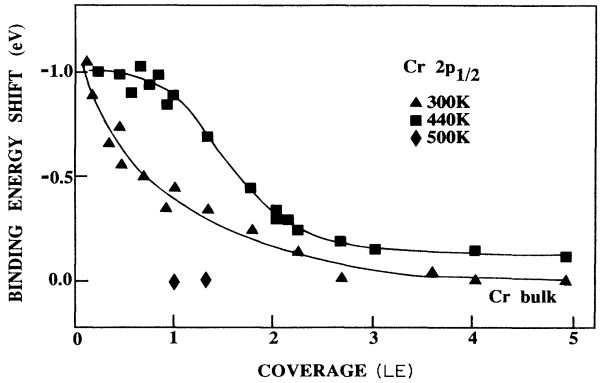

FIG. 4. Binding-energy shift of the Cr 2*p* core level (referred to bulk Cr) vs coverage of Cr deposited on Ag(100) held either at RT or at 440 K during deposition. Also shown is the data point for 1 LE deposited at 500 K.

noteworthy that the BE of the additional structure is close to that of the surface state (0.65 eV) observed on clean Cr(100).[15] The present interpretation is also consistent with the conclusion of Ref. 10 that an inhomogeneous layer, with coexistence of poorly ordered monolayer and bilayer islands, is formed at RT.

The drastic difference in the submonolayer growth mode between deposition at RT and 440 K is also illustrated in Figs. 2 and 3 by the very different evolutions of the Cr 3*d* features versus coverage. In contrast with the 440-K data, drastic changes in shape and location of the Cr 3*d* emission versus coverage is apparent at RT. In particular, this means that the Cr environment in the overlayer changes progressively with coverage, i.e., the growth mode is more complex at RT than at 440 K. More specifically by 0.1 LE only one narrow peak is visible at 1.15 eV. It is due to mostly isolated Cr adatoms present at this stage and can be interpreted as a virtual bound state.[9,16] By 0.25 LE the spectrum becomes similar to the 440-K data at 1 LE (Fig. 2). One observes a broader structure where two major components near 1.07 and 1.5 eV can be distinguished. This broadening and splitting reflects the lateral interaction of Cr adatoms in 2D islands formed with increasing coverage. Upon further deposition, by 0.5 LE, no major qualitative change takes place except an overall enhancement and blurring of the emission in the 0–3-eV BE range. Yet, by 0.8 LE the additional emission just below E_F reveals the presence of Cr in bilayer sites and, in turn, the inhomogeneous nature of the layer grown at RT.

Further support of this picture comes from Fig. 4, which compares the evolution of the Cr 2*p* core-level BE vs Cr coverage for RT and 440-K deposition. At RT the rapid increase in BE toward the bulklike value again indicates a drastic change in the Cr environment and coordination in the submonolayer range and more generally up to ~4 LE. In contrast, at 440 K the BE change is initially very small up to 1 LE, of the order of the experimental uncertainty. This is the expected behavior if the Cr layer formed at 440 K grows in the form of 2D islands, since most of the Cr adatoms incorporated in such islands have the same monolayer coordination whatever the coverage in the 0–1-LE range. The small (~0.1 eV) change in BE actually observed might be due to island edge effects, the importance thereof decreasing with island size and thus with coverage. Alternatively, the defects always present on the real Ag(100) surface may induce small deviations from ideal layer-by-layer growth mode. Obviously above 1 LE, even at 440 K, the monolayer coordination must evolve toward a bulklike configuration by filling of bilayer or multilayer sites and the BE must change rapidly toward the value measured in Cr bulk, as observed experimentally. As can be seen in Fig. 4, according to the above picture, at RT the Cr coordination is always more bulklike than at 440 K. In the submonolayer range this confirms the occupation of bilayer sites at RT. Finally, let us note that deposition of 1 LE at 500 K results in a bulklike Cr 2*p* BE, as expected if agglomeration into 3D islands occurs at this temperature.

Concluding this section, we observe that the present Cr 3*d* and Cr 2*p* photoemission studies are entirely consistent with the unusual growth mode of Cr on Ag(100) in the monolayer range found in Ref. 10. We have been able to identify the Cr 3*d* valence-band signature of Cr in a monolayer and Cr in bilayer or multilayer platelets, i.e., to establish a relationship between atomic and electronic structure. In summary, at RT with increasing coverage up to 1 LE, characteristic Cr 3*d* photoemission signatures reveal initially isolated Cr adatoms, then a large density of poorly ordered monolayer islands, and finally bilayer platelets which coexist with the monolayer domains. Possibly the structure of such layers may be described by random deposition models[17] because of a low adatom mobility at RT. As expected from thermodynamics, the enhanced mobility of the adatoms at high (>460 K) temperatures induces Cr agglomeration into 3D islands. Yet, at moderate (~440 K) substrate temperatures there is now ample evidence that only 2D islands are formed up to 1 LE and, thus, a flat ordered monolayer with characteristic Cr 3*d* states can be prepared.

C. Experimental band structure of the Cr monolayer

We turn now our attention to the ordered Cr monolayer prepared by deposition at 440 K. Figure 5 displays the evolution of the characteristic Cr 3*d* features at normal emission with the polar angle of incidence α of the He I ($\hbar\omega=21.2$ eV) photons. As noted in Sec. III B for $\alpha=45°$, besides the dominant peak at 1.07 eV the rough data exhibit a broad shoulder near 1.5 eV. It can be seen that both components show a different behavior versus light incidence angle. While the 1.07-eV peak shows little change versus light incidence angle the intensity of the component near 1.50 eV is strongly reduced near normal incidence ($\alpha=18°$). This indicates that the 1.07- and 1.5-eV structures are excited by the component of the light polarization vector **A**, respectively parallel and normal to the surface. According to the selection rules at normal emission[18] the states at 1.05 eV must have $\bar{\Gamma}_5$ ($d_{xz,yz}$) symmetry. As can be seen in Fig. 5, this feature is completely dominant for Ne I excitation, where it is observed at the same BE, as it should be for a true 2D electronic state. Note also that for a given $k_{\parallel}$, the parallel component of the wave vector (here $k_{\parallel}=0$), this state is well defined in energy, since its width, after deconvolution of the experimental resolution, is less than 200 meV. Inverse hole lifetimes of this order of magnitude seem quite consistent with a 3*d* derived surface state of ~1-eV BE. The spectrum for $\alpha=20°$ indicates that, besides this dominant $\bar{\Gamma}_5$ state, a single feature at ~1.5 eV cannot represent the high-BE side of the Cr 3*d* emission. There are actually two components located at 1.40 and 1.75 eV, as shown by the fit in Fig. 5. The component at 1.75 eV is rather small and is comparable to the 1.40-eV feature only near normal incidence of light. Thus, we attribute the 1.40-eV component to a $\bar{\Gamma}_1$ ($d_{3z^2-r^2}$) state because of its typical dependence of light incidence. The small feature at 1.75 eV must then reflect emission from either a $\bar{\Gamma}_3$ ($d_{x^2-y^2}$) or $\bar{\Gamma}_4$ (d_{xy}) state, which is forbidden at strict normal emission, but may be observed experimentally because of the finite acceptance cone of the analyzer. Thus, at normal emission, we actually identify two dominant components at 1.07 and 1.40 eV with $\bar{\Gamma}_5$ and $\bar{\Gamma}_1$ symmetry, respectively, as expected theoretically if the Cr layer has fourfold symmetry.[18]

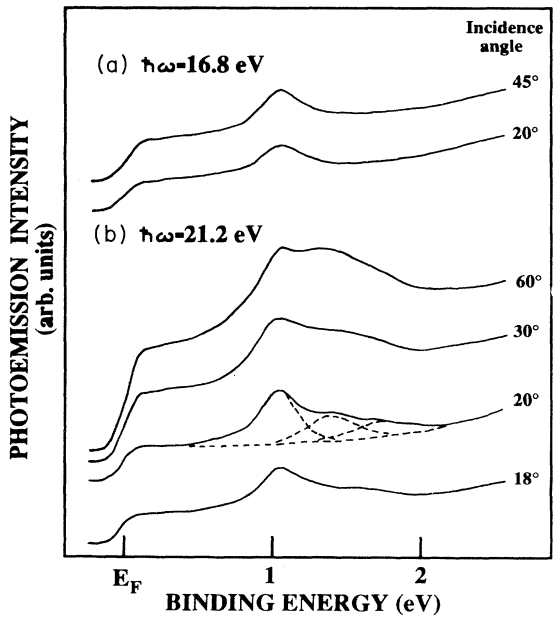

FIG. 5. Influence of light incidence angle α (referred to surface normal) on the intensity of the Cr 3*d* features observed at normal emission from 1 LE of Cr deposited at 440 K for two different photon energies: (a) $\hbar\omega=16.8$ eV and (b) $\hbar\omega=21.2$ eV. A fit of three components to the Cr 3*d* structure observed at $\alpha=20°$ is also shown.

Figure 6 shows an example of the dispersive behavior of the Cr 3*d* derived states versus polar angle of emission. These spectra, which are collected with $\hbar\omega=21.2$-eV excitation in the Ag(010) azimuthal plane, probe the $\bar{\Sigma}$ symmetry line of the SBZ (Fig. 7). As can be seen, usually up to three Cr 3*d* features with a small but measurable dispersion can be identified. Some peaks due to direct transitions from Ag 5*s* bulk band are indicated by arrows. The relevant experimental band dispersions along $\bar{\Sigma}$, inferred from the data of Fig. 6 and from similar data taken at different photon energies or light incidence angles, are shown in Fig. 7. In the determination of $k_{\parallel}(E)$ we have used the measured work function of the Ag(100) surface coated with a Cr monolayer: $\Phi=4.26$ eV. This is 140±20 meV lower than clean Ag(100). Similarly, spectra collected in the Ag(001) azimuth plane yield the band dispersions along $\bar{\Delta}$ shown in Fig. 8. Clearly there is good agreement between the $E(k_{\parallel})$ obtained with He I and Ne I photons. The periodicity in reciprocal space as well as the extremal behavior at $\bar{\Gamma}$ and $\bar{M}$ is also well marked, in particular for the upper band having $\bar{\Gamma}_5$ symmetry at $\bar{\Gamma}$, which can be easily followed through the whole SBZ. This testifies to the 2D character of the Cr 3*d* derived bands and, in turn, of the Cr layer prepared in this work. The fact that up to three resolved bands with Cr 3*d* character can be identified experimentally is a favorable situation due to the small hybridization with Ag bulk bands. The Ag 5*s* band has a very low density of states at the Cr 3*d* energies, and the latter are located more than 2 eV above the top edge of the Ag 4*d* bands. Finally, we note that similar measurements for 0.5-LE Cr deposited at 440 K yield exactly the same 2D band structure as in Figs. 7 and 8. This band structure is characteristic of monatomic Cr islands on Ag(100).

D. Evidence of antiferromagnetism

Figure 9 shows the calculated bands expected for a paramagnetic transition metal arranged in a 2D square lattice.[19] The dispersion of the major bands derived from *d* states can be understood in terms of simple tight binding considerations. For instance, the d_{xz}, d_{yz} derived bands along $\bar{\Gamma}\bar{M}$ show antibonding character at $\bar{\Gamma}_5$ and bonding character at $\bar{M}_5$ as a result of the signs of the overlapping orbital lobes. On the other hand, $d_{3z^2-r^2}$ ($d_{x^2-y^2}$) derived bands are bonding at $\bar{\Gamma}_1$ ($\bar{\Gamma}_3$) and antibonding at $\bar{M}_1$ ($\bar{M}_3$). This characteristic dispersion be-

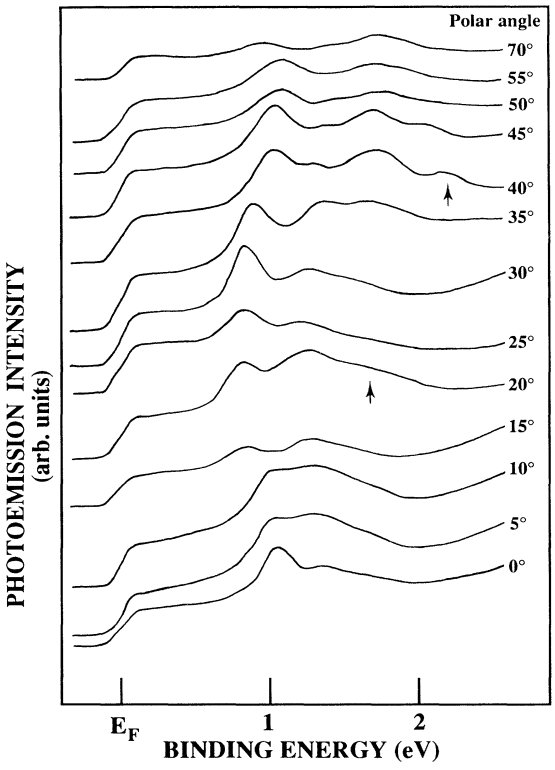

FIG. 6. Typical set of angle-resolved spectra for 1 LE deposited at 440 K showing the dispersion of the Cr 3*d* features vs polar angle. The collection plane and photon energy are the same as in Fig. 1 and the light incidence angle is 30°. These spectra probe the $\bar{\Sigma}$ symmetry line of the SBZ. The arrows indicate direct transitions from Ag 5*s* bulk band.

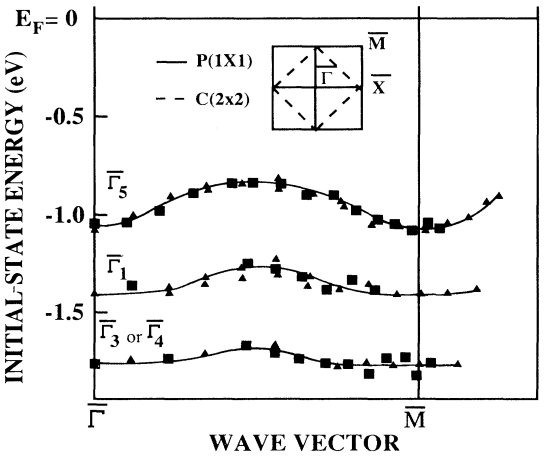

FIG. 7. Experimental two-dimensional band structure along the $\bar{\Sigma}$ ($\bar{\Gamma}\bar{M}$) symmetry line of the $p(1\times1)$ paramagnetic SBZ for a Cr monolayer on Ag(100). The photon energy is 21.2 eV (▲) and 16.8 eV (■). The inset shows the $p(1\times1)$ and $c(2\times2)$ SBZ. The orbital character of the bands at $\bar{\Gamma}$ is $d_{xz,yz}$ (1.07 eV), $d_{3z^2-r^2}$ (1.40 eV), and d_{xy} or $d_{x^2-y^2}$ (1.75 eV).

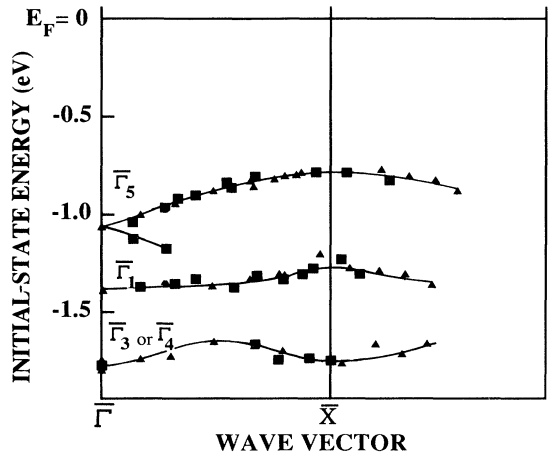

FIG. 8. Same as in Fig. 7 but along the $\bar{\Delta}$ ($\bar{\Gamma}\bar{X}$) symmetry line of the $p(1\times1)$ SBZ.

havior near $\bar{\Gamma}$ and $\bar{M}$ is preserved in more realistic calculations for a 3*d* metal monolayer supported by a noble-metal substrate.[20] Yet it can be seen than the experimental bands show bonding character at $\bar{\Gamma}_5$. Moreover, for a half-filled *d*-shell metal such as Cr, the Fermi energy E_F must be located near the middle of the *d* bands. Thus $\bar{\Gamma}_5$ should be unoccupied in paramagnetic Cr, and *d*-band states should exist in the neighborhood of E_F. Experimentally, there is no evidence of *d* bands crossing the Fermi level, and there is actually a gap in the *d* states of 0.8 eV below E_F. Also, the observed dispersions are much smaller than expected from a paramagnetic Cr monolayer. For instance, the experimental width of the $d_{xz,yz}$ bands along $\bar{\Sigma}$ is about 240 meV as compared to ~1.0 eV calculated for the similar Fe/Ag(100) system.[20] Hence, it is quite clear that the observed band topology is not compatible with the one expected from a paramagnetic Cr monolayer. A similar reasoning leads to the

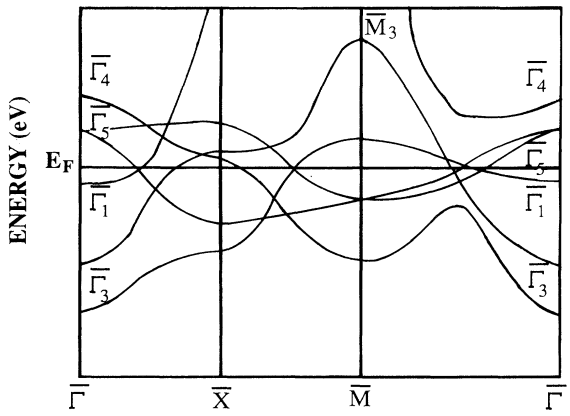

FIG. 9. Calculated band structure for a paramagnetic transition metal on a square lattice (Ref. 19). The indicated Fermi energy is an approximate position for the Cr case with half-filled *d* bands.

conclusion that a ferromagnetic configuration of the Cr layer does not explain the observed bands either. Again, the essential arguments are that ferromagnetism would result in a much larger total bandwidth (about 2.5 eV for a given spin, similar to the paramagnetic bandwidth) and a substantial density of states at E_F as shown by the calculations of Ref. 6.

Actually, the data suggest that the Cr monolayer must be stabilized by some mechanism which opens a large gap at E_F. According to the general theorem of Ref. 7, in the Cr case one expects a tendency towards the formation of a twofold superlattice either by reconstruction, lattice distortion, or by antiferromagnetism. Interestingly, it can be seen that the observed bands actually indicate a $c(2\times2)$ superstructure rather than a simple $p(1\times1)$ translation symmetry. There is nearly a perfect symmetry of the bands, in particular for the upper one, about the midpoint of the $\bar{\Sigma}$ line in the $p(1\times1)$ SBZ. There is very good agreement in the location of the Cr $3d$ levels observed at $\bar{\Gamma}$ and $\bar{M}$, which are thus equivalent points of the actual reciprocal space. The relationship between reduced $c(2\times2)$ and primitive $p(1\times1)$ zone is depicted in Fig. 7.

The following analysis shows that the observed band topology can be at least qualitatively understood in terms of a tight-binding model for the d bands of an isolated Cr layer arranged in a square lattice with two sublattices of inequivalent sites, say a spin-up and a spin-down site, as shown in the inset of Fig. 10. For an isolated layer, hybridization between $d_{xz,yz}$ and $d_{3z^2-r^2}$ or $d_{x^2-y^2}$ does not occur because of their different symmetries. Let us consider, for instance, the odd $d_{xz,yz}$ band along $\bar{\Sigma}$. As pointed out above, in a $p(1\times1)$ square lattice this band shows a dispersion opposite to the experimental one near $\bar{\Gamma}$. For a $c(2\times2)$ superstructure with a two-atom basis, an elementary tight-binding model taking only nearest-neighbor interactions into account yields the following two bands for a given orbital (for instance, odd $d_{xz,yz}$) along $\bar{\Sigma}$:

$$E=\pm[\Delta^2+16\gamma^2\cos^2(q\pi/2)]^{1/2}\ ,$$

where $\pm\Delta$ are the diagonal terms on the two inequivalent sites (in the case of an antiferromagnet $\pm\Delta$ is the alternating exchange potential seen by an electron of a given spin on the spin-up and spin-down sites of the lattice); γ is a hopping integral, and $0\le q\le1$ for wave vectors between $\bar{\Gamma}$ and the midpoint of $\bar{\Gamma}\bar{M}$. The symmetry labels are relevant to the $p(1\times1)$ SBZ shown in Fig. 7, i.e., in the case of an antiferromagnet, the SBZ for the chemical or crystallographic unit cell.

The two bands are drawn in Fig. 10 for different values of Δ. For $\Delta=0$ one merely gets the paramagnetic band, folded back into the reduced zone. For $\Delta\neq0$ but small with respect to the paramagnetic bandwidth 8γ a small gap appears near the new zone boundary at the midpoint of $\bar{\Gamma}\bar{M}$. For large $\Delta\sim8\gamma$ the paramagnetic band is split into two much flatter bands well separated in energy. For a half-filled d shell, $E_F=0$ in this simple model, so that the lower band is occupied and the upper band is empty. Clearly, the occupied band closely resembles the

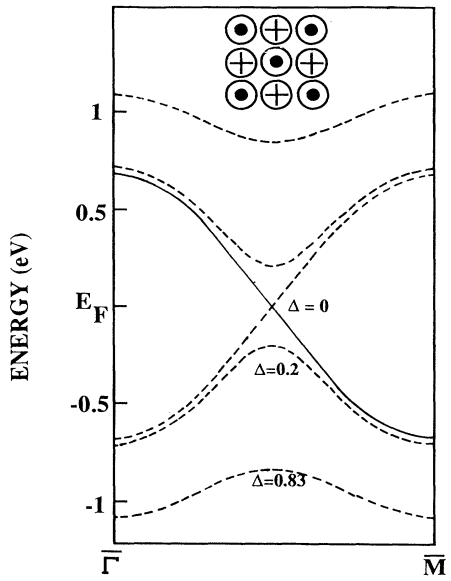

FIG. 10. Tight-binding bands along $\bar{\Sigma}$ (for a given d orbital) of a transition metal on a square lattice with two sublattices of spin-up and spin-down atoms (as shown in the inset) for different values of Δ. $\pm\Delta$ are the diagonal elements for an electron on the two inequivalent sites relative to the zero of the energy scale which coincides with the Fermi energy for half-filled bands, and γ is a hopping integral. The symmetry labels are the paramagnetic $p(1\times1)$ SBZ. The values $\Delta=0.83$ eV and $\gamma=0.17$ eV were obtained from a fit to the experimental $d_{xz,yz}$ bands. The relevant unfolded paramagnetic ($\Delta=0$) band is shown as a solid line.

experimental $d_{xz,yz}$ band along $\bar{\Sigma}$. In particular, it displays the right dispersion behavior. A good fit to the experimental band is obtained for $\Delta\sim0.83$ eV and $8\gamma\sim1.36$ eV. The latter value appears to be physically reasonable since it is comparable to the calculated $d_{xz,yz}$ bandwidth for a ferromagnetic (or paramagnetic) Fe layer on Ag(100).[20] On the other hand, Δ indicates a large energy gain and stabilization by forming a twofold superlattice in the Cr monolayer. Note that the electronic energy is strongly reduced over the whole reciprocal space and not just near the $c(2\times2)$ zone boundary. Physically, the drastic reduction in bandwidth from ~1.4 eV to ~240 meV stems from the strongly repulsive potential on the nearest neighbors. For a given spin, the wave function of the occupied (unoccupied) band is largely concentrated on atoms with the same (opposite) spin orientation, i.e., on next-nearest neighbors whose overlap is very small. Qualitatively, the shape near $\bar{\Gamma}$ of the two other bands observed along $\bar{\Sigma}$ can be understood in the same way. Note that within the above model, whatever the dispersive behavior of the original paramagnetic band, the lower split part for $\Delta\neq0$ always disperses upward when moving away from $\bar{\Gamma}$, as observed experimentally. This results in the curious parallel dispersions of all bands along $\bar{\Sigma}$. According to the paramagnetic band shapes in Fig. 9 and the model in Fig. 10 the lowest experimental

band observed along $\bar{\Sigma}$, in particular near $\bar{\Gamma}$ (or $\bar{M}$) must have d_{xy} or $d_{x^2-y^2}$ symmetry or both, in agreement with our analysis of light polarization effects. However, it appears that while the fit to the experimental $d_{xz,yz}$ band yields a paramagnetic bandwidth $8\gamma \sim 1.4$ eV of the right order of magnitude, this is not the case for the lower $d_{x^2-y^2}$ band. The relative magnitude of the $d_{xz,yz}$ and $d_{x^2-y^2}$ bandwidths can be estimated from the data in Fig. 9. Due to the larger overlap it appears that for $d_{x^2-y^2}$ $8\gamma \sim 2.5$ eV (Ref. 20), whereas a fit to experiment yields a much lower value $8\gamma = 0.6$ eV. In other words, for the lowest band along $\bar{\Sigma}$ the expected dispersion (~ 500 meV) is larger than measured (~ 100 meV).

Nevertheless, the present simple picture is capable of accounting, in a physically transparent way, for the major features of the experimental bands along $\bar{\Sigma}$, namely, their $c(2\times 2)$ symmetry, their small dispersions, and, most important, the presence of a large gap in the Cr $3d$ states at E_F. Qualitatively, experimental bands along $\bar{\Delta}$ may be obtained by folding the paramagnetic bands along $\bar{X}\bar{M}$ over $\bar{\Gamma}\bar{X}$ and opening large gaps at band crossings. A more quantitative analysis of the data by means of realistic calculations, which, in particular, take into account the hybridization effects in the Cr layer interacting with the Ag(100) substrate, is in progress and will be reported elsewhere.[21]

The above discussion is based on the example of an antiferromagnetic superstructure. Yet, by just changing the meaning of Δ and γ the above model would describe a $c(2\times 2)$ reconstruction or lattice distortion as well. Hence, at this point, we can only conclude that photoemission indicates a drastic stabilization effect which drives the paramagnetic $p(1\times 1)$ layer into a more stable state with a $c(2\times 2)$ superstructure. When considered along with the LEED observations of Sec. III A, the possibility of a stabilization by a mechanism of structural origin appears, however, not to be tenable. As pointed out above, the large value of Δ implies that the electrons in the Cr layer see a strong potential of $c(2\times 2)$ symmetry. If the superstructure were due to reconstruction or lattice distortion the potential seen by the electrons would be the direct Coulomb potential. Hence a $c(2\times 2)$ pattern with intense half-order spots should be observed by LEED in a wide range of primary beam energies. In particular, it seems very difficult to understand why, except below 30 eV, the LEED pattern is merely $p(1\times 1)$. Yet LEED and photoemission can be reconciled if we assume that the Cr monolayer is indeed a strong antiferromagnet. The low-energy d electrons feel then a large spin-dependent exchange potential which accounts for the experimental bands. On the other hand, backward scattering of high-energy (≥ 20 eV) LEED electrons by the exchange potential is known to be quite weak.[22] Tamura, Blügel, and Feder predict small extra-beam intensities of about 1% of the (10) integral order beam in the low (~ 40 eV) primary-beam energy range decreasing rapidly at higher energies.[23] This compares favorably with our LEED observations, since we indeed observe a weak $c(2\times 2)$ pattern in 20–30-eV range with an intensity of the $(\frac{1}{2}\frac{1}{2})$ spots relative to the (10) spots of $\sim 2\%$ at 26 eV. From this LEED and photoemission evidence we conclude that the Cr monolayer actually adopts the configuration of a strong antiferromagnet. According to our LEED observations this magnetic state persists at least up to 430 K, i.e., close to those temperatures above 450 K where the metastable Cr monolayer agglomerates into 3D clusters.

A rough estimation of the strength of the antiferromagnetic stabilization can be made from the observed band structure. In the above model, the energy gap is $2\Delta = 1.70$ eV for the upper $d_{xz,yz}$ bands. This compares favorably with the gap of ~ 2 eV in the local density of states for spin-up and spin-down states calculated for the antiferromagnetic Cr monolayer on Pd(100).[6] Since in mean-field theory Δ is proportional to the staggered magnetization it is apparent that the actual magnetic moment on the Cr must be close to the calculated moments of $3.46\mu_B$ on[6] Pd(100) or $3.48\mu_B$ on[5] Au(100). Actually, there is further evidence from the data at hand that Cr carries a large local moment of the order of $4\mu_B$. First, note that it has been established that isolated Cr adatoms on (or in) Ag or Au exhibit a local moment of this order of magnitude.[8,9,16,24] As can be seen in Fig. 4 the Cr $2p$ BE's measured for isolated Cr adatoms (low coverage limit for RT deposition) and Cr embedded in the monolayer are identical within experimental uncertainty. The BE is about 1.0 eV lower than for Cr in bulk environment. Essentially the same shift was observed in our previous work on the Cr/Au(100) system,[8] where it was shown that this indicates a substantial ($\sim 0.2e$) $s \rightarrow d$ charge transfer for Cr in (or on) Au(100) with respect to the bulk atomic configuration $d^{5-\varepsilon}s^{1+\varepsilon}$. Hence, the configuration evolves towards the free-atom $d^5s^1(^6S)$ ground-state configuration which carries a large magnetic moment. There is apparently a close relationship between atomic configuration (and, in turn, the Cr $2p$ BE) and local magnetic moment. At any rate, the similarity in the Cr $2p$ BE strongly suggests that Cr in the monolayer actually carries a magnetic moment very similar to the isolated adatom local moment. In contrast, note the rapid change in BE toward the Cr bulk value in the case of RT deposition where bulklike atomic configurations with probably a much lower local moment are formed in the submonolayer range.

The electronic structure of isolated adatoms can be described by the Friedel-Anderson virtual bound-state model[25,26] in the magnetic case. In previous studies,[9,16] it was shown that the occupied majority spin states give rise to the photoemission feature visible at 1.15 eV in the spectra collected at very small Cr coverages (see Fig. 3). For Cr incorporated into the monolayer on Ag(100) the interatomic distance (2.88 Å) is still large with respect to the atomic spacing in bulk (2.49 Å). This suggests that the isolated adatom local moment might well be largely preserved in the monolayer. Indeed the observed band structure of the monolayer can be interpreted as the result of a small interaction between virtual bound states of neighboring adatoms. This induces a small splitting (~ 400 meV) and dispersion (~ 300 meV) of the occupied majority spin d states but there is apparently no fundamental change in the electronic structure of the Cr with

respect to the original magnetic virtual bound-state picture of an isolated Cr adatom. First-principles calculations for a Cr impurity in Ag by Podloucky, Zeller, and Dederichs[24] gives a majority- minority spin peak splitting of 3.2 eV with a local moment of $4.2\mu_B$. This is not very different from the splitting of ~ 3 eV obtained in Ref. 6 for Cr in the monolayer. Obviously, both experiment and theory show that an isolated Cr adatom on or Cr impurity in Ag and Cr in the monolayer have similar energy locations and splittings of their spin-up and spin-down local densities of states and thus similar local moments. This also suggests that the intra-atomic Coulomb repulsion between opposite spins U is ~ 3 eV for Cr in the monolayer. Clearly the observed dispersions are small with respect to U and the correlation effects must be very strong. Thus, one may question the validity of a single-particle picture for the description of the electronic structure. Experimentally the one-hole states are rather well defined in energy and $k_{\parallel}$, at least for the upper bands of $d_{xz,yz}$ character. The tight-binding bands invoked in the above discussion can be considered as a Hartree-Fock approximate solution to the 2D Hubbard model on a square lattice for the interacting electrons. It is generally agreed that the true ground state in a half-filled single-band Hubbard model is an antiferromagnetic insulator as predicted by mean-field theory but the antiferromagnetism is overestimated because of the neglect of spin and charge fluctuations.[27] A possible effect of the correlations may be a reduction of the dispersions predicted by a band model. In this respect, note that the measured dispersion of the $d_{x^2-y^2}$ band is apparently smaller than expected.

Finally, let us mention that there is evidence of multiplet splittings in the Cr $3p$ and other core levels. Since the origin of core-level multiplet splittings in metals may be quite complex, these data will be reported and discussed elsewhere.[28] We merely note here that multiplet splitting may be caused by the exchange interaction, which leads to a difference in energy between final states with the spin of the core hole parallel or antiparallel to the $3d$ spin. Since the observed splitting is very large (~ 2 and 6 eV for Cr $3p$), this is a further hint of the presence of a large local moment on Cr in the monolayer.

IV. CONCLUSION

We have confirmed the possibility of preparing a Cr monolayer with a good degree of perfection by slow (0.50 LE/min) deposition on a mildly (~ 440 K) heated Ag(100) substrate. LEED and photoemission strongly suggest that the layer is a 2D antiferromagnet. Although the arguments are rather compelling, they are still indirect and we cannot, at this point, definitely rule out other possible interpretations of the data, for instance, a different mechanism stabilizing the Cr monolayer. Apparently, few experiments may provide direct evidence of the antiferromagnetic configuration. A promising method is magnetic scanning tunneling microscopy, which takes advantage of the spin dependence of the tunneling current. The feasibility of such experiments has been demonstrated recently on the Cr(100) surface by using a ferromagnetic CrO_2 tip.[29] Another possible technique is spin-polarized photoelectron diffraction in core-level emission which has provided valuable information in the case of bulk antiferromagnets.[30] At low photoelectron takeoff angles the sensitivity of this method might be sufficient to determine the local magnetic structure in the monolayer. At any rate the present finding opens the possibility to study a clean-model case of 2D magnetism with the challenge to develop new appropriate experimental methods.

Finally, if a monatomic Cr platelet on Ag(100) actually adopts an antiferromagnetic configuration, this is expected to play a major role in the initial mode of growth. From a magnetic point of view, chemisorption of a Cr adatom in bilayer positions, i.e., on top of a monatomic Cr island, necessarily results in a locally frustrated spin configuration with the concomitant complex behavior. At some stage in the subsequent growth process the antiferromagnetic arrangement of the first layer must switch to a ferromagnetic one, albeit weaker, since this is the magnetic structure within a (100) atomic plane in the bulklike spin arrangement of Cr and bcc Cr reportedly grows on Ag(100).[10] At least in the monolayer the magnetism is strong; thus we anticipate that the magnetic contribution to the total energy of a given atomic configuration should be important. In particular, for deposition in the monolayer range, one expects a competition between magnetic stabilization which favors large interatomic distances as in the ordered flat monolayer and ordinary chemical bond stabilization which favors short interatomic distances as in Cr bulk. There is experimental evidence[11] that magnetic effects indeed control the initial growth mode of Cr on Ag(100).

ACKNOWLEDGMENTS

The Laboratoire de Physique et de Spectroscopie Electronique is "Unité associée au Centre National de la Recherche Scientifique No. 1435."

[1]P. A. Dowben, M. Onellion, and Y. J. Kime, Scanning Microsc. **2**, 177 (1988).
[2]H. Ohtani, C. T. Kau, M. A. Van Hove, and G. A. Somorjai, Prog. Surf. Sci. **23**, 155 (1986).
[3]C. Lui, E. R. Moog, and S. D. Bader, Phys. Rev. Lett. **60**, 2422 (1988).
[4]C. L. Fu, A. J. Freeman, and T. Oguchi, Phys. Rev. Lett. **54**, 2700 (1985).
[5]A. J. Freeman and C. L. Fu, J. Appl. Phys. **61**, 3356 (1987).
[6]S. Blügel, M. Weinert, and P. H. Dederichs, Phys. Rev. Lett. **60**, 1077 (1988).
[7]V. Heine and J. H. Samson, J. Phys. F **13**, 2155 (1983).
[8]M. C. Hanf, C. Pirri, J. C. Peruchetti, D. Bolmont, and G. Gewinner, Phys. Rev. B **39**, 3021 (1989).

[9]D. A. Newstead, C. Norris, C. Binns, and P. C. Stephenson, J. Phys. C **20**, 6245 (1987).
[10]C. Krembel, M. C. Hanf, J. C. Peruchetti, D. Bolmont, and G. Gewinner Phys. Rev. B **44**, 8407 (1991).
[11]C. Krembel, M. C. Hanf, J. C. Peruchetti, D. Bolmont, and G. Gewinner (unpublished).
[12]C. Krembel, M. C. Hanf, J. C. Peruchetti, D. Bolmont, and G. Gewinner, J. Magn. Magn. Mater. **92**, 529 (1991).
[13]T. S. Padmore, G. Thornton, and P. A. Padmore, Solid State Commun. **67**, 163 (1988).
[14]U. König, S. Blügel, G. Hörmandinger, and P. Weinberger, Solid State Commun. **76**, 1309 (1990).
[15]G. Gewinner, J. C. Peruchetti, A. Jaegle, and R. Pinchaux, Phys. Rev. B **27**, 3358 (1983).
[16]M. C. Hanf, L. Haderbache, P. Wetzel, C. Pirri, J. C. Peruchetti, D. Bolmont, and G. Gewinner, Solid State Commun. **68**, 113 (1988).
[17]J. W. Evans, Phys. Rev. B **43**, 3897 (1991).
[18]J. Hermanson, Solid State Commun. **22**, 9 (1977).
[19]D. Wang, A. J. Freeman, and H. Krakauer, Phys. Rev. B **29**, 1665 (1984).
[20]R. Richter, J. G. Gay, and J. R. Smith, J. Vac. Sci. Technol. A **3**, 1498 (1985).
[21]G. Allen, Phys. Rev. B (to be published).
[22]P. W. Palmberg, R. E. De Vames, and L. A. Vredevoe, Phys. Rev. Lett. **21**, 682 (1968).
[23]E. Tamura, S. Blügel, and R. Feder, Solid State Commun. **65**, 1255 (1988).
[24]R. Podloucky, R. Zeller, and P. H. Dederichs, Phys. Rev. B **22**, 5777 (1980).
[25]J. Friedel, Can. J. Phys. **34**, 1190 (1956).
[26]P. W. Anderson, Phys. Rev. **124**, 41 (1961).
[27]J. E. Hirsch, Phys. Rev. B **31**, 4403 (1985).
[28]C. Krembel, M. C. Hanf, J. C. Peruchetti, D. Bolmont, and G. Gewinner (unpublished).
[29]R. Wiesendanger, H. J. Güntherodt, G. Güntherodt, R. J. Gambino, and R. Ruf, Phys. Rev. Lett. **65**, 247 (1990).
[30]B. Sinkovic, D. J. Friedman, and C. S. Fadley, J. Magn. Magn. Mater. **92**, 301 (1991).